Robust Position Control of A Continuum Manipulator Based on Selective Approach and Koopman Operator

Haodong Wang[1,2,3] , Wenyu Liang[2], *Member, IEEE*, Boyuan Liang[2], Hongliang Ren [3,4], *Senior Member, IEEE*, Zhijiang Du[1], *Member, IEEE*, Yan Wu[2], *Senior Member, IEEE*

***Abstract*—Continuum manipulators have infinite degrees of freedom and high flexibility, making it challenging for accurate modeling and control. Some common modeling methods include mechanical modeling strategy, neural network strategy, constant curvature assumption, etc. However, the inverse kinematics of the mechanical modeling strategy is difficult to obtain while a strategy using neural networks may not converge in some applications. For algorithm implementation, the constant curvature assumption is used as the basis to design the controller. When the driving wire is tight, the linear controller under constant curvature assumption works well in manipulator position control. However, this assumption of linearity between the deformation angle and the driving input value breaks upon repeated use of the driving wires which get inevitably lengthened.This degrades the accuracy of the controller. In this work, the Koopman theory is used to identify the nonlinear model of the continuum manipulator. Under the linearized model, the control input is obtained through model predictive control (MPC). As the lifted function can affect the effectiveness of the Koopman operator-based MPC (K-MPC), a novel design method of the lifted function through the Legendre polynomial is proposed. To attain higher control efficiency and computational accuracy, we use a selective control scheme according to the state of the driving wires. When the driving wire is tight, the linear controller is employed; otherwise, the K-MPC is adopted. Finally, a set of static and dynamic experiments have been conducted using an experimental prototype. The results demonstrate high effectiveness and good performance of the selective control scheme.**

***Index Terms*—Continuum manipulator, Koopman operator, constant curvature assumption, model predictive control, nonlinear system.**

I. Introduction

With the advancement in control technology and new material, the development of continuum manipulators increasingly gathers traction. Compared with traditional industrial robots, continuum manipulators have the characteristics of small volume, lightweight, structural compliance and flexibility [1]. These traits are important for the application scenarios that require safe human-robot interaction, such as surgical [2] and rescue [3] robotics. Due to the deformable nature of the continuum manipulator, controller design is a challenge [4]. The control algorithms of continuum manipulators can be summarized into two categories: model-based and model-free methods.

In model-based methods, the physical structure of the continuum manipulator is analyzed to design a system model [5]. The common control methods of the continuum manipulator involve force control and angle control of the motor, which divide the model-based methods into mechanical modeling strategy and constant curvature assumption. Under mechanical modeling strategy, the principle of virtual power [6], Cosserat rod theory [7], Timoshenko beam [8] etc., are adopted to analyze the continuum manipulator's deformation. Then, using the D-H method, forward kinematics can be derived through the obtained deformation angle [9]. However, inverse kinematics is hard to obtain, making the controller design difficult. Moreover, the generalization of this method is poor. On the other hand, under the constant curvature assumption approach, the continuum manipulator's deformation is assumed to be an arc for easy calculation of its kinematics [10]. The effectiveness of the constant curvature assumption is verified by 1-degree-of-freedom (1-DoF) and multi-DoF continuum manipulators [11], [12]. Therefore, considering the feasibility of the master-slave algorithm for continuum manipulators, angle control of the motor is commonly used in model-based method. Nevertheless, it is further assumed that the continuum manipulator's driving wires are tight in this modeling process. A common driving method of the continuum manipulator is the wire-driven mode. The driving wire is made of ductile steel wire ropes which causes the 'slack' problem against usage. Using the Da Vinci surgical robotics system as the reference of a typical wire-driven robot, its instruments need to be repaired after 10 surgical procedures [13]. After the driving wire is slack, the effectiveness of the constant curvature assumption will deteriorate and affect the control system performance (i.e., precision and accuracy).

On the other hand, the model-free methods use the data-driven approach [14]. For example, machine learning is used to

This research is supported by the National Natural Science Foundation of China under Grant No. U1813213, the Hong Kong Research Grants Council (RGC) Collaborative Research Fund under grant No. CRF C4026-21GF, the China Scholarship Council under grant No. 202106120121, and in part by the A*STAR Robotic Horizontal Technology Coordinating Office Seed Fund under grant No. C211518005. (Corresponding authors: *Zhijiang Du* and *Hongliang Ren*.)

[1] State Key Laboratory of Robotics and System, Harbin Institute of Technology, Harbin, China 150080.

[2] Institute for Infocomm Research (I2R), A*STAR, Singapore 138632.

[3] Department of Biomedical Engineering, National University of Singapore, Singapore 117575.

[4] Department of Electronic Engineering, Shun Hing Institute of Advanced Engineering, The Chinese University of Hong Kong, Hong Kong, China 999077

design the controller without making any physical assumption [15]. The data set required for controller design is collected when the continuum robot is in good operating condition. Ho *et al.* designed a soft robot and a learning-based controller [16]. Due to the uncertainty of the operating environment, the online inverse kinematic model is obtained by a non-parameter learning method. In [17], a pneumatic serial-parallel soft robot is developed by Lakhal *et al.* and its inverse kinematics is calculated through geometric methods. Since its forward kinematics is difficult to express explicitly, it is trained through a neural network. However, the mapping relationship between input and output is a 'black-box' and may not guarantee convergence.

Comparing the above control methods, it is noted that the constant curvature assumption has advantages in terms of computational efficiency and algorithm implementation. When the driving wire is tight, the relationship between the motor angle and the deformation angle of the continuum manipulator is linear. When the driving wire is slack, the accuracy of the constant curvature assumption decreases because the slack of the driving wire breaks the linear relationship between the length of the driving wires and the motor angle. This results in nonlinearity between the motor angle and the continuum manipulator's deformation angle. An effective solution to this problem is to identify this nonlinear relationship. Machine learning-based approaches can be a good solution. However, global convergence may not be guaranteed [18]. An alternative data-driven approach is K-MPC. The key to the K-MPC is the linearization of the nonlinear model by Koopman theory, which is for the nonlinear model. Moreover, the essence of the Koopman theory is that the finite-dimensional nonlinear system can be lifted to an infinite-dimensional linear system. In this way, the information of the original system can be retained. In practice, computing an infinite-dimensional Koopman operator is not achievable. Therefore, a finite-dimensional approximation of the operator is carried out through extended dynamic mode decomposition (EDMD) [19]. Based on the EDMD method, the global linearization of a nonlinear system can be realised with experimental or simulation data, which consists of control input and other information about the nonlinear system. Based on the linearized model constructed under the Koopman theory, the control input of the system can be obtained through MPC [20]. The MPC solves a convex optimization problem, which can converge to a specific solution. Therefore, a data-driven controller can be constructed by the K-MPC method. In addition to reducing computational and feedback complexity, the K-MPC controller could perform better than the controller constructed directly through the original nonlinear system. K-MPC has been successfully applied to control various robots, such as robotic fish [21] and soft robots [22], [23]. The difficulty in designing the K-MPC is the selection of the lifted function of the Koopman theory. For example, in [22], [23], the polynomials with a maximum degree of two were selected as the lifted function. The trajectory tracking accuracy is poor based on such lifted functions.

Since the mechanical modeling strategy has low applicability with its inverse kinematics being difficult to obtain while the machine-learning-based approach requires a large amount of training data without convergence guarantee, we propose to use the constant curvature assumption as the basis for the controller design in this work. When the driving wire is tight, a controller of the continuum manipulator can be constructed using the linear relationship of the angles. However, many works ignore the slack problem of the driving wires which degrades the accuracy of the controller. This nonlinear relationship needs to be identified so as to improve accuracy. To linearize this nonlinear relationship, Koopman theory is adopted. Based on the linearized model constructed by the Koopman theory, the control input is obtained through MPC. Therefore, by using the K-MPC, the controller of the continuum manipulator can be constructed. Since the lifted function affects the effectiveness of the K-MPC, in this work, a novel design method of the lifted function through the Legendre polynomial is proposed. The designed lifted function solves the problem of low control accuracy in [22], [23]. To the best of our knowledge, no prior art discussions on a Koopman operator-based framework that solves the control problem due to the slack of driving wires. Compared with mechanical modeling strategies, this K-MPC is not affected by the configuration of the continuum manipulator, this algorithm can be reused by reacquiring experimental data. Moreover, the K-MPC requires much less data as compared to machine-learning-based approaches, and its convergence can be guaranteed by the eigenvalues of the Koopman operator. To attain higher control efficiency and computational accuracy, a selective control scheme is proposed according to the state of the driving wires: when the driving wire is tight, use the linear controller under the constant curvature assumption; otherwise, K-MPC is adopted. On the premise of ensuring control accuracy, this selective control scheme can reduce the maintenance times of the continuum manipulator. It also improves the operational efficiency of the controller.

In this paper, the main contributions include:

- This is the first work to investigate and analyze the effects of the driving wire's states (especially when it is slack) on the system modeling and control performance of the continuum manipulator.
- A position controller using the Koopman theory and MPC is designed to deal with the issues due to system nonlinearity when the driving wire is slack. Therein, a novel design method of the lifted functions for the Koopman operator through the Legendre polynomial is proposed.
- To attain higher control efficiency and computational accuracy, a selective control scheme according to the state of the driving wires is proposed.

The rest of this paper is organized as follows. In Section II, we summarize the structure of the continuum manipulator. Next, the selective control scheme is proposed in Section III. An experimental setup is constructed. The effectiveness of the proposed selective control scheme is verified in Section IV. Discussion is given in Section V. Finally, Section VI concludes this paper.

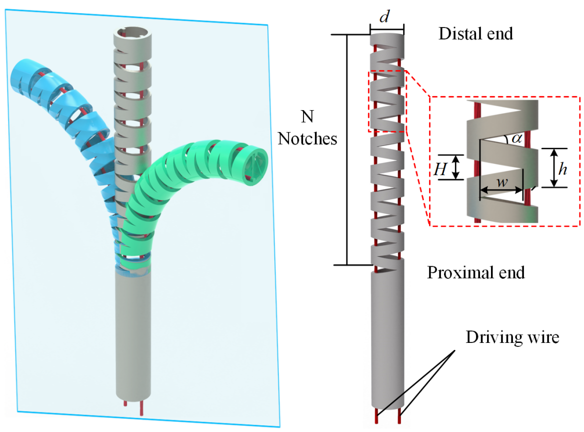

Fig. 1. Schematic diagram of the underactuated wire-driven continuum manipulator.

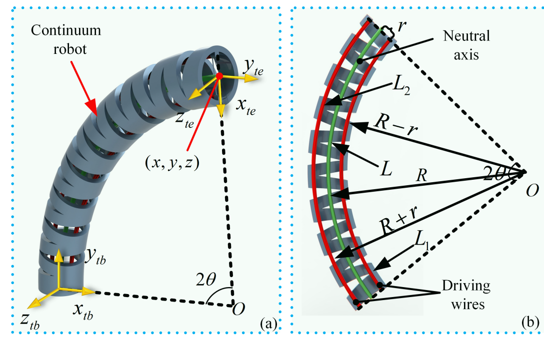

Fig. 2. Kinematic analysis of the continuum manipulator: (a) the kinematic coordinate system, (b) the calculation of the driving input value of the motor.

II. Overview of The Structural Analysis

In this section, the structure of the underactuated wire-driven continuum manipulator is summarized. The schematic diagram of the continuum manipulator is shown in Fig. 1. Nitinol alloy, which has the characteristics of super-elasticity, fatigue resistance, and structural strength, is selected as the material of the continuum manipulator. Triangular notches are machined on the Nitinol alloy tube through wire-cutting technology. The outer and inner diameters of the continuum manipulator are 10 mm and 8.8 mm, respectively. The internal cavity of the continuum manipulator is reserved to provide channels for electrical wires and driving wires for other joints.

The continuum manipulator, which has 1-DoF, is driven by two wires. One end of the driving wire is fixed at the distal end, and the other end is transmitted to the proximal end, as shown in Fig. 1. The result is an under-actuated continuum robot actuated in the form of a marionette. The two wires are separated by 180°. That is, applying tension to the right wire causes the continuum manipulator to bend to the right, and applying tension to the left wire causes the continuum manipulator to bend to the left.

III. Selective Control Scheme Design

As previously discussed, the drawback of a machine-learning-based strategy lies in its requirement for enormous amount of data and its inability to guarantee convergence. The mechanical modeling strategy can obtain higher control accuracy. However, this strategy is only suitable for specific robots; and it is difficult to obtain the inverse kinematics via this strategy. Nevertheless, inverse kinematics is essential in the master-slave control of the continuum manipulator. The constant curvature assumption has advantages in terms of computational efficiency and algorithm implementation in comparison to other algorithms. Therefore, the constant curvature assumption is used as the basis for the controller. However, the control accuracy is affected by the state of the driving wire. To solve this issue, a selective controller is designed in this section. The state of the driving wire is used as the judgment condition of the selective controller. With this selective approach, the operation efficiency of the controller can be improved.

A. Linear Model-Based Control (Method 1)

The constant curvature assumption is often employed to develop the control algorithm for the continuum manipulator with verified effectiveness. The kinematic coordinate system of the continuum manipulator is shown in Fig. 2(a). The base coordinates $\{tb\} = \{\ x_{tb} \quad y_{tb} \quad z_{tb}\ \}$ is set at the center of the proximal end face. The x_{tb}-axis points to the center of the bend and the y_{tb}-axis is perpendicular to the proximal end face. The end coordinate system $\{te\} = \{\ x_{te} \quad y_{te} \quad z_{te}\ \}$ is set at the center of the distal end face. The x_{te}-axis points to the center of the bend and the y_{te}-axis is perpendicular to the distal end face. Others axes are determined through the right-hand grip rule.

The continuum manipulator's neutral axis is assumed to be its central axis. The constant curvature assumption is employed to construct kinematics. The continuum manipulator's shape is equivalent to an arc, and the central angle of the curved circle is 2θ. Using the geometric relationship, the distal position (P) is obtained as

$$P = \begin{bmatrix} R(1-\cos(2\theta)) \\ R\sin(2\theta) \\ 0 \end{bmatrix} = \frac{L}{2\theta}\begin{bmatrix} 1-\cos(2\theta) \\ \sin(2\theta) \\ 0 \end{bmatrix}, \quad (1)$$

where R and L are the radius of curvature and the length of the continuum manipulator, respectively.

The transformation from the base coordinate system $\{tb\}$ to the end coordinate system $\{te\}$ is achieved through the following process. The base coordinate system $\{tb\}$ moves $R\sin(2\theta)$ along the y_{tb}-axis, then moves $R(1-\cos(2\theta))$ along the x_{tb}-axis, and finally rotates 2θ along the z_{tb}-axis to obtain the end coordinate system $\{te\}$. The coordinate transformation matrix is constructed as follows,

$$\begin{array}{l} T = \mathrm{Trans}(y, R\cdot\sin(2\theta))\cdot \\ \mathrm{Trans}(x, R\cdot(1-\cos(2\theta)))\cdot\mathrm{Rot}(z, 2\theta) \end{array}. \quad (2)$$

The inverse kinematics is established as follows. When the distal position (x, y) is given, the manipulator's deformation angle (2θ) is calculated as

$$2\theta = 2\arcsin(\frac{x}{\sqrt{x^2+y^2}}). \quad (3)$$

Accoding to the known deformation angle (2θ), the length (L_i) of the driving wire is defined as follows,

$$L_i = 2\theta(R + (-1)^i r), i = 1, 2, \tag{4}$$

where i indicates the i-th driving wire.

According to (4), the length changes (ΔL_i) of the i-th driving wires are calculated as follows,

$$\Delta L_i = L_i - L = 2\theta(R + (-1)^i r) - 2\theta R = (-1)^i 2r\theta. \tag{5}$$

When the driving wires are tight, the relationship between the motor angle (ΔM) and the length change of the driving wire is linear. Based on (5), the relationship between the motor angle and the deformation angle is defined,

$$\Delta M = \Delta L_i / R_1 = (-1)^i 2r\theta / R_1, \tag{6}$$

where R_1 is the radius of the reel. Here, (6) is called "Method 1", which is one control scheme of continuum manipulator.

Based on the above equations, the mapping relationship among driving space (motor angle), joint space (deformation angle of continuum manipulator), and Cartesian space (distal positions) is established. It is obvious that Method 1 is linear. However, after long-term use of the continuum manipulator, the driving wires are slack, making the relationship between the length of the driving wires and the motor angle nonlinear, i.e., (6) becomes nonlinear. This nonlinear relationship reduces the accuracy of the control scheme under the constant curvature assumption. To retain the accuracy of the control scheme, the nonlinear relationship between the motor angle and the deformation angle should be identified.

B. Koopman Operator-based Model Predictive Control (K-MPC)

In system control, the model uncertainty is usually eliminated by robust control and adaptive control. However, these methods are dependent on the model. To deal with the above problems, data-driven technology is gradually emerging. The data-driven Koopman theory is used to identify the nonlinear relationship between the deformation angle and the motor angle in this section.

1) Construction of Linearized Model by Koopman Operator: In the finite-dimensional nonlinear system, all scalar functions of its state space have an equivalent infinite-dimensional linear representation, called Koopman operator. The essence of the Koopman theory is that the linearization of a nonlinear system is achieved through lifting the original system.

In measurement space, a discrete-time nonlinear controlled dynamic system is defined by

$$\dot{x}(t) = F(x(t), u(t)), \tag{7}$$

where $u(t) \in U \subset \mathbb{R}^m$ and $x \in X \subset \mathbb{R}^n$ are the system input and system output, respectively; F is the mapping function of the system; and X, U are compact subsets. $\phi_t(x_0)$ is the solution of (7) at the initial value x_0 and time t.

The linearization process of the Koopman theory is shown in Fig. 3. Based on the lifted function φ, an infinite-dimensional function space $\mathcal{F}$ $(f, \mathbb{R}^m, \mathrm{K})$ can be constructed through the state (X, M, F) of system. The element of function space $\mathcal{F}$ is

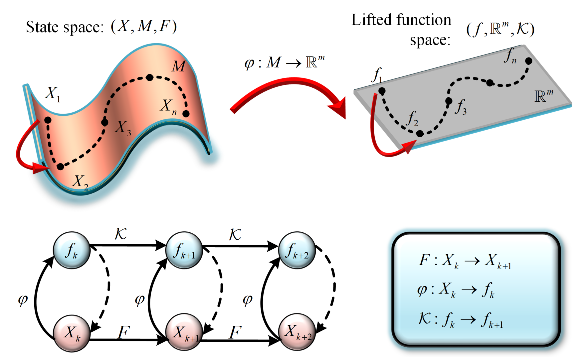

Fig. 3. Linear evolution of Koopman theory.

called observable f. The evolution of the observable f along system trajectory can be described by Koopman operator $\mathcal{K}: \mathcal{F} \to \mathcal{F}$. The linear operator $\mathcal{K}$, which is infinite-dimensional, is defined as follows,

$$\mathcal{K}f = f \circ \phi_t, \tag{8}$$

where $\circ$ describes a combination of functions.

The Koopman operator $\mathcal{K}$ can describe a dynamical system, even if the system is nonlinear. For any observable f_1, f_2 on the infinite-dimensional function space, we have the following equation,

$$\begin{aligned} \mathcal{K}(\alpha f_1 + \beta f_2) &= \alpha f_1 \circ \phi_t + \beta f_2 \circ \phi \\ &= \alpha \mathcal{K} f_1 + \beta \mathcal{K} f_2 \end{aligned}, \tag{9}$$

where $\alpha, \beta \in \mathbb{R}$.

Based on the Koopman operator in an infinite-dimensional space, a linearization of a nonlinear system can be obtained. However, this linear representation cannot be described by a finite-dimensional matrix. To enable explicit representation, EDMD is used to project the Koopman operator into a finite-dimensional subspace. Based on the obtained observation data, the finite-dimensional approximation of the Koopman can be carried out. $\overline{\mathcal{F}} \subset \mathcal{F}$, which is composed of $N > n + m$ linearly independent basis functions $\{\varphi_i : \mathbb{R}^m \times \mathbb{R}^n \to \mathbb{R}\}_{i=1}^N$, is defined as a subspace of $\mathcal{F}$. The lifted function of subspace $\overline{\mathcal{F}}$ is described through basis functions,

$$\varphi(x, u) = \begin{bmatrix} \varphi_1(x, u) & \ldots & \varphi_N(x, u) \end{bmatrix}^T, \tag{10}$$

where $\varphi(x, u)$ is called as the lifted function.

The linear combination of basis functions can express each observable $\overline{f} \in \overline{\mathcal{F}}$. To provide a vector expression of observable $\overline{f} \in \overline{\mathcal{F}}$, coefficient $\alpha = \begin{bmatrix} \alpha_1 & \ldots & \alpha_N \end{bmatrix}^T$ is defined. When the state x and input u are given, the observable can be defined as follows,

$$\overline{f} = \alpha^T \cdot \varphi(x, u). \tag{11}$$

Based on the vector representation of observable, that is, (11), the linear operator on the subspace $\overline{\mathcal{F}}$ is expressed as a $N \times N$ matrix. Therefore, the Koopman operator $\overline{\mathcal{K}}$ can be approximated through limited experimental data. The function of the linear operator $\overline{\mathcal{K}}$ is valid for any observable. Based on (8) and (11), the following equation can be constructed

$$\alpha^T \cdot \overline{\mathcal{K}}^T \cdot \varphi(x, u) = \alpha^T \cdot \varphi(\phi(x, u), u). \tag{12}$$

Based on the matrix transform of (12), the best approximation $\overline{\mathcal{K}}$ of the Koopman operator is calculated as,

$$\overline{\mathcal{K}} = \varphi^T(x,u)^\dagger \cdot \varphi^T(\phi(x,u),u). \tag{13}$$

To obtain an approximate value of Koopman operator $\overline{\mathcal{K}}$ from discrete experimental data, the k-th discrete measurements are constructed as "snapshot pairs" $(c[k], d[k], u[k]); k \in [1, K]$.

$$\begin{array}{l} c[k] = x[k] \\ d[k] = \phi(x[k], u[k]) \end{array}, \tag{14}$$

where $x[k]$ represents the output of the k-th measurement, $u[k]$ is the constant input between $c[k]$ and $d[k]$.

Based on the lifted functions $\varphi(x,u)$, two $K \times N$ matrices are constructed through the K snapshot pairs.

$$\psi_c = \left[\begin{array}{c} \varphi(\ c[1] \quad u[1]\ )^T \\ \dots \\ \varphi(\ c[K] \quad u[K])^T \end{array} \right], \tag{15}$$

$$\psi_d = \left[\begin{array}{c} \varphi(\ d[1] \quad u[1]\ )^T \\ \dots \\ \varphi(\ d[K] \quad u[K])^T \end{array} \right]. \tag{16}$$

Based on the constructed matrices ψ_c and ψ_d, the linear operator $\overline{\mathcal{K}}$ can be obtained through the minimized optimizer,

$$J = \frac{1}{2} \min \sum_{k=1}^{K} \left\| \psi_d(k,:) - \psi_c(k,:) \cdot \overline{\mathcal{K}} \right\|^2. \tag{17}$$

The above equation is a least squares problem. It must have either a global minimum or a family of vectors in the solution space. Regularization may need to be carried out to obtain the unique solution [24]. Therefore, $\overline{\mathcal{K}}$ that minimizes the above equation is obtained,

$$\overline{\mathcal{K}} = G^\dagger D, \tag{18}$$

where $\dagger$ represents the pseudo-inverse of a matrix,

$$\begin{array}{l} G = \frac{1}{K} \sum\limits_{k=1}^{K} \psi_c(k,:)^T \psi_c(k,:) \\ D = \frac{1}{K} \sum\limits_{k=1}^{K} \psi_c(k,:)^T \psi_d(k,:) \end{array}, \tag{19}$$

with $G, A \in \mathbb{R}^{N \times N}$.

When an initial state and control input are given, we are looking for a predictor, which is suitable for linear control design methods such as MPC [25]. The form of the predictor is built as follows,

$$\begin{array}{l} z[i+1] = Az[i] + Bu[i] \\ x[i] = Cz[i] \end{array}, \tag{20}$$

where $x\,[i]$ is the i-th output of the system, $z[i] \in \mathbb{R}^N$ is the state, $u\,[i]$ is the i-th input of the system, and $A \in \mathbb{R}^{N \times N}$, $B \in \mathbb{R}^{N \times m}$, $C \in \mathbb{R}^{n \times N}$.

To construct a linear operator in the form of (20), the functions of the system output are used as the first $N-p$ basis functions. The remaining p basis functions are selected as the elements of the system input. Based on the selected basis functions, the Koopman operator is calculated by (18). The selected basis functions are constructed as follows,

$$\begin{array}{l} \varphi_i(x,u) = Y_i(x); i \in [1, ..., N-p] \\ \varphi_i(x,u) = u_i; i \in [N-p+1, ..., N] \end{array}, \tag{21}$$

where $Y: \mathbb{R}^n \to \mathbb{R}$, u_i is the i-th element of the input u.

The first n selected basis functions are the same as each output component in this work, i.e.,

$$Y_i(x) = x_i; i \in [1, n], \tag{22}$$

where $n < (N-p)$.

Based on (22), the transformation matrix C from the state space to the output space is obtained,

$$C = \left[I_{n \times n}, 0_{n \times (N-n)} \right]. \tag{23}$$

Based on (14) and (21), the cost function (17) can be modified to the following form,

$$J1 = \frac{1}{2} \min \sum_{i=1}^{K} \left\| \left[\begin{array}{c} Y(d[k]) \\ u[k] \end{array} \right] - \overline{\mathcal{K}}^T \left[\begin{array}{c} Y(c[k]) \\ u[k] \end{array} \right] \right\|^2, \tag{24}$$

where $Y(x) = \left[\begin{array}{ccc} Y_1(x) & \dots & Y_{N-p}(x) \end{array} \right]^T$.

To construct the form of (20), z is the same as $Y(x)$, i.e., $z = Y(x)$. Based on the obtained experimental data, the minimized optimizer is used to calculate A and B. Then, the cost function becomes

$$J2 = \frac{1}{2} \min \sum_{i=1}^{K} \| Y(d[k]) - A \cdot Y(c[k]) - B \cdot u[k] \|^2. \tag{25}$$

By comparing the cost functions $J1$ and $J2$, A and B of the predictor can be embedded in the matrix $\overline{\mathcal{K}}^T$. On the basis of obtaining the Koopman operator with experimental data, A and B of the predictor can be obtained through the separation matrix $\overline{\mathcal{K}}^T$.

$$\overline{\mathcal{K}}^T = \left[\begin{array}{cc} A_{(N-p) \times (N-p)} & B_{(N-p) \times p} \\ \dots & \dots \end{array} \right]. \tag{26}$$

The stability of the Koopman theory can be judged by the eigenvalues of (18). These eigenvalues are affected by the design method of the lifted function. Therefore, the lifted function and data processing procedures used in this paper are given below. The state and input of the system are the manipulator's deformation angle (2θ) and the motor angle (ΔM), respectively. The obtained experimental data which is the continuum manipulator's deformation angle is normalized by the maximum value (e). The lifted function is set according to (21), the processed experimental data (x), and the Legendre polynomial.

$$\begin{array}{l} \varphi(x,u) = \\ e * \left[\begin{array}{ccccccc} x & P_1(x) & \dots & P_i(x) & \dots & P_N(x,u) & u/e \end{array} \right]^T, \end{array} \tag{27}$$

where u is the system input, $e * x$ is the system state, $P_i(x)$ is the i-th order Legendre polynomial.

2) Linearized Model Predictive Control: The driving wires are slack during the long-term use of the continuum manipulator which produces a nonlinear relationship between the motor angle and the length change of the driving wire. That means the relationship between the motor angle and the deformation angle of the continuum is nonlinear. In this work, Koopman theory is used to linearize this nonlinearity. Then, a linear predictor, used to design a model-based controller, can be obtained through the Koopman operator. Based on the obtained linear predictor, we look for a model-based controller to obtain the system input. MPC is one commonly-used model-based control technique. The control input is obtained by solving an open-loop optimal control problem in the finite time domain at each sampling.

The optimization problem of MPC consists of a cost function, a system model, and constraints. The system model obtained by the Koopman operator is linear. Then, the cost function is designed based on the obtained linearized model. A control scheme obtained by optimizing the cost function is used to control the nonlinear system. Since the system model is linear, the solution of MPC is a convex quadratic programming problem. At each sampling, a unique optimal sequence of inputs over a finite-time horizon can be solved through the following equation,

$$
\begin{aligned}
&\min V(\{u[i], z[i]\}_{i=1}^{N}) = \\
&\sum_{i=1}^{N} (Cz[i] - x[i])^T Q[i] (Cz[i] - x[i]) + u[i]^T R[i] u[i] \\
&s.t. z[i+1] = Az[i] + Bu[i], i \in [1, N] \\
&E[i]z[i] + F[i]u[i] \leq b[i], i \in [1, N] \\
&z[1] = Y(x[k])
\end{aligned}
, \qquad (28)
$$

where $N \in \mathbb{N}$ is the prediction horizon, $Q[i] \in \mathbb{R}^{(N-p)\times(N-p)}$ and $R[i] \in \mathbb{R}^{p\times p}$ are real symmetric matrices, $E[i] \in \mathbb{R}^{c\times(N-p)}$ and $F[i] \in \mathbb{R}^{c\times p}$ are parameter matrices with respect to z and u, $b \in \mathbb{R}^{c}$ is the bounding constraints. When the program is called, the current lifted state $Y(x[k])$ is used to initialize $z[1]$.

The K-MPC method is summarized as follows. Based on (27), the lifted function is established. Then, the nonlinear system is linearized through (18) and the lifted function. Based on the linearized model, the system input is calculated by (28). Moreover, the concepts used in MPC are given as follows. The control horizon is the number of the control sequence, i.e., the number of the control value. The predictive horizon is the number of the lifted state. The predictive horizon can be greater than or equal to the control horizon. The outputs of the control horizon are the motor angles. The outputs of the predictive horizon are the lifted states, obtained by the lifted function. Since the first selected basis function is the system output, the effect of prediction can be evaluated.

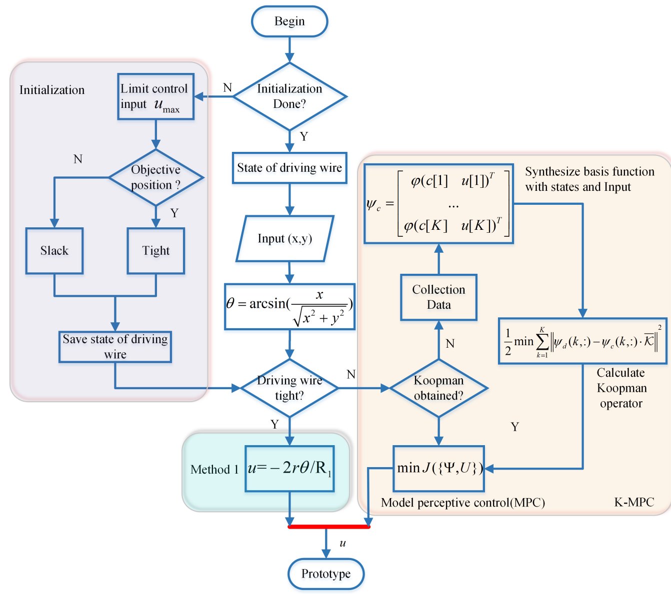

Fig. 4. Flow chart of the selective control scheme.

TABLE I
DESIGN PARAMETERS OF THE CONTINUUM MANIPULATOR

d	α	H	w	h
10 mm	20 °	2.73 mm	4 mm	1.64 mm

C. Selective Control Scheme

The proposed selective control scheme is shown in Fig. 4. The control system initialization of the continuum manipulator needs to be executed before usage. The initialization method is summarized as follows. The maximum input $u_{\max}$ is inputted into the control system. According to the acquired distal position, the state of the driving wire is judged. A selective control scheme is proposed according to the obtained state of the driving wire. When the state of the driving wire is tight, Method 1 is adopted, otherwise, the K-MPC method is adopted. The usage of the K-MPC method is introduced as follows. First, the algorithm verifies whether the Koopman operator is obtained. If yes, the input of the system is directly calculated through MPC. Otherwise, experimental data are collected. Based on the lifted function and the experimental data, the Koopman operator is calculated by (18). Then, the MPC method is executed. This selective control scheme can reasonably utilize the control resources.

IV. PRELIMINARY EXPERIMENT

In this section, the prototype is built on basis of the designed continuum manipulator. Under the different states of the driving wire, these two proposed algorithms (Method 1 and K-MPC) are verified, respectively.

A. Experimental Setup

The experimental setup is constructed, as shown in Fig.5, which comprises a continuum manipulator, a light source, a camera (Intel RealSense Depth Camera D435), and driving devices. The continuum manipulator contains 8 triangle notches on one side, that is, the total notch number is 16. The design

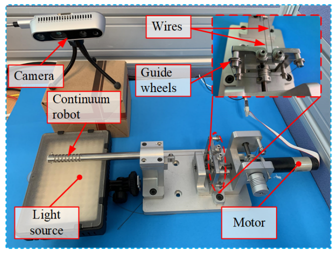

Fig. 5. Experimental setup for the continuum manipulator.

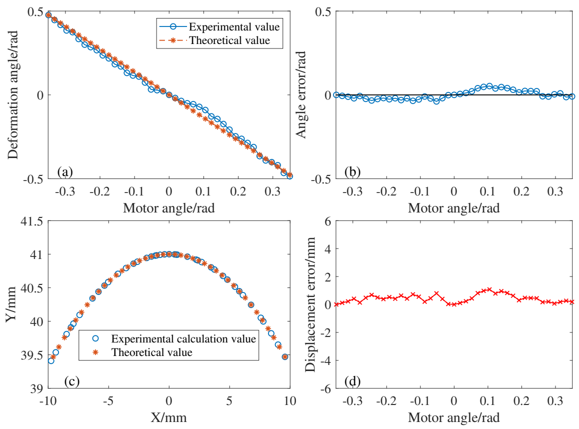

Fig. 6. The test results under the tight state of the driving wires: (a) is the theoretical deformation angle vs. experimental angle; (b) is the angle error; (c) is the theoretical position vs. experimental calculation position; (d) is the displacement error.

parameters of the continuum manipulator shown in Fig. 1 are given in Table I. The transmission method of the driving wires is shown in Fig.5. Those wires are connected to the motor through guide wheels. The control mode of the continuum manipulator is based on the position control of the motor. The control input u and the system state are the motor angle (ΔM) and the manipulator's deformation angle (2θ), respectively. The camera is used to capture the manipulator's movement. Based on the obtained images, the data are calculated through Halcon software (MVTec, Germany).

B. Method 1 Validation

When the state of the driving wire is tight, the effectiveness of Method 1 is verified. And the experiment of the driving wire slack is tested in the subsequent subsection. When the motor rotates, one of the driving wires is loaded, making the continuum manipulator produce plane bending. The motor angle is from $-\frac{\pi}{9}$ to $\frac{\pi}{9}$ rad with an increment of $\frac{\pi}{180}$ rad. The test results of the tightened driving wires are shown in Fig.6. The theoretical deformation angle vs. experimental angle is shown in Fig. 6(a). The data have good linearity. And the maximum absolute angle error is 0.0526 rad. The distal positions are calculated based on the obtained deformation angles and constant curvature assumption. The experimental calculation positions vs. theoretical positions are compared in Fig.6 (c). The maximum displacement error is 1.0775 mm, as shown in Fig.6 (d).

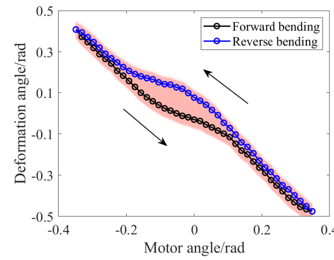

Fig. 7. Data for nonlinear system identification

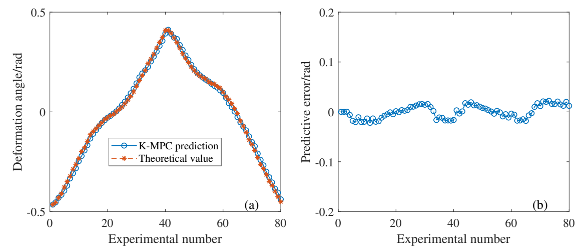

Fig. 8. One-step predicted results of using the Koopman operator: (a) one-step predicted state based on the Koopman operator; (b) the error of the predictive state.

C. Data Collection and System Identification

After the long-term use of the continuum manipulator, the driving wires are slack, making the relationship between the length of the driving wires and the motor angle exhibit nonlinearity. It makes the relationship between motor angle and the manipulator's deformation exhibit nonlinearity. A data-driven K-MPC is used to identify this relationship. The data collection and the parameter identification of the K-MPC algorithm with the slack of the driving wire are performed in this subsection.

The limit deformation angle (2θ) is about $\pm\frac{\pi}{6}$ rad. To avoid damage to the continuum manipulator, the pulses of the motor are controlled from - 20000 to 20000 by the laptop with a step of 1000. The control signal is defined as

$$v = \begin{cases} 1000x - 20000, x \in [0, 40] \\ -1000x + 60000, x \in [40, 80] \end{cases}. \tag{29}$$

This experiment is carried out nine times, and the average values are used as the experimental data. The relationship between the deformation angle and the motor angle corresponding to control signal v is shown in Fig.7. It can be seen that there is a large hysteresis between the deformation angle and the motor angle. The interval with the smaller hysteresis is precisely the interval with the larger motor angle from Fig.7. Since the motor rotates at a certain angle, the driving wire is re-tensioned in this interval. It is concluded from Fig. 7 that using Method 1 to control the continuum manipulator can result in a large error.

This nonlinear model of the continuum manipulator is identified by the Koopman theory. To ensure algorithm convergence, the maximum order of the Legendre polynomial in (27) is set as 28. Based on the obtained experimental data and lifted function, the Koopman operator $\overline{\mathcal{K}}$ is identified through (18). Fig.8 shows the one-step predicted state of the Koopman

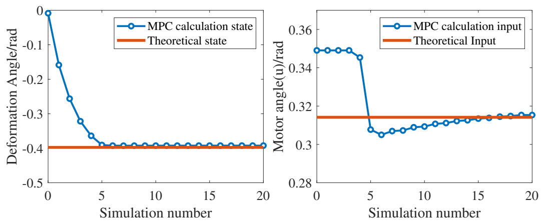

Fig. 9. Verification of the K-MPC Algorithm: (a) is the predictive result of state Vs the reference state; (b) is the predictive input Vs the reference input.

operator. It can be concluded from Fig.8 (a) that the Koopman theory has a good predictive effect. The error of the predicted state is from -0.0221 to 0.0222 rad, as shown in Fig.8 (b).

After the Koopman operator is obtained, the MPC algorithm is verified. The parameters of (28) is set as follows: $Q = [5], R = [0.1]$ and prediction horizon $N = 20$. The receding horizon is set as 20. The initial state and objective state of the system are set as -0.0085 and -0.3975 rad, respectively. Fig. 9 depicts the predictive output and control output after each receding optimization, where the horizontal axis is the number of the receding horizon, i.e., the simulation number. The predictive and theoretical states are -0.3924 and -0.3975 rad, respectively. The predictive and theoretical inputs are 0.3153 and 0.3142 rad, respectively. The error rate of input is 0.35%. The K-MPC algorithm can accurately achieve the predictive task.

D. Control Comparison: Method 1 vs. Nonlinear Algorithms

When the state of the driving wire is slack, experiments are constructed to compare the predictive effect of Method 1 and nonlinear algorithms (neural network and K-MPC). To show the superiority of K-MPC in nonlinear algorithms, a neural network model is constructed. Based on the MATLAB Neural Network Fitting Toolbox, the model is trained through 80 sets of experimental data. The input and output of the model are the deformation angle and the motor angle, respectively. The training algorithm is set as Levenberg-Marquardt. The hidden neurons' number is set as 10.

A reference trajectory (cosine function), set as the deformation angle of the continuum manipulator, is used to test the effectiveness of the model under dynamic driving. Based on the reference trajectory, the motor angles are calculated through Method 1, neural network, and K-MPC algorithm, respectively. The obtained motor angle is used to control the continuum manipulator. When the manipulator's deformation is stable, the data is collected through the experimental setup. The reference trajectory is defined by,

$$Def\_angle = -\left(\frac{210}{11}\right)^{\circ} \cdot \cos(\frac{\pi}{18}i), \tag{30}$$

where Def_angle is the deformation angle, i is the i-th step.

The data obtained from the above methods are compared with the reference trajectory, as shown in Fig. 10, where the horizontal axis is the step number. The absolute errors between theoretical and actual data are given to show the effect of different algorithms. The results show that the accuracy of the nonlinear model prediction algorithms is better than the linear model algorithm (Method 1). The K-MPC algorithm is superior to the neural network, as shown in Fig.10.

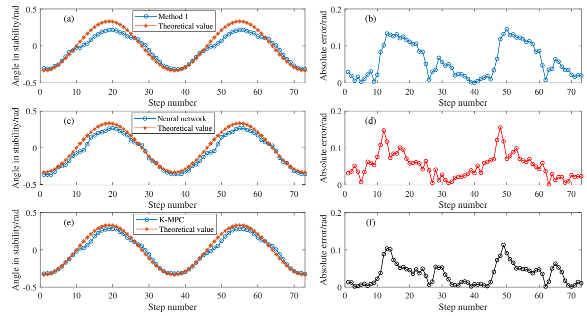

Fig. 10. Comparison of different control algorithms: (a) and (b) are the data obtained from Method 1 Vs objective function and absolute error, respectively; (c) and (d) are the data obtained from neural network model Vs objective function and absolute error, respectively; (e) and (f) are the data obtained from K-MPC model Vs objective function and absolute error, respectively.

TABLE II
ANGLE ERROR OF DIFFERENT CONTROL ALGORITHMS

State of wire	Algorithm	Average error(rad)	standard deviation
Slack	Method 1	0.0594	0.0458
Slack	Neural network	0.0523	0.034
Slack	K-MPC	0.0345	0.0286
Tight	Method 1	0.0211	0.0138

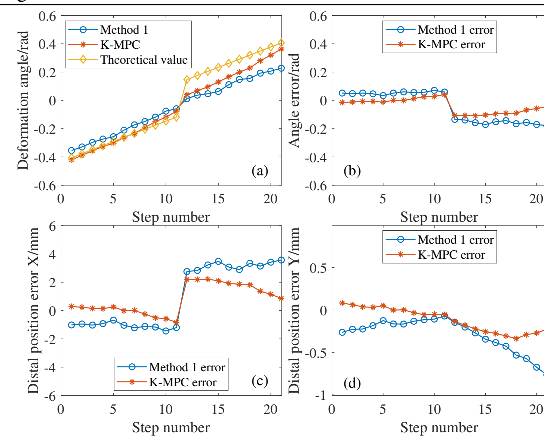

Fig. 11. Comparison of Method 1 and K-MPC: (a) and (b) are the comparison of deformation angles and angle error, respectively; (c) and (d) are the comparison of distal position error in the x and y direction, respectively.

Based on the above-mentioned experiments in subsections B and D, the average angle errors and standard deviations of the different algorithms are calculated, as shown in Table II. The result shows that the accuracy of the K-MPC algorithm in the slack state of the driving wire is close to Method 1 in the tight state of the driving wire. Therefore, the selective control algorithm is efficient.

E. Control Comparison: Method 1 vs. K-MPC

When the state of the driving wire is slack, control strategies between K-MPC and Method 1 are compared in this subsection. Based on the distal position of the continuum manipulator, the deformation angle is calculated by (3). Then, the motor angles are calculated through Method 1 and the

K-MPC. Based on the obtained motor angles, the continuum manipulator is driven. The experimental data are collected. The distal positions can be obtained based on the obtained deformation angle and constant curvature assumption. Twenty-one sets of distal positions are randomly selected for this test. The results are shown in Fig.11. The maximum absolute angle errors of Method 1 and K-MPC are 0.1788 and 0.1089 rad, respectively. Compared with Method 1, the error of the K-MPC algorithm is reduced by 39%. The maximum position errors in the x direction of Method 1 and K-MPC are 3.5717 and 2.2196 mm, respectively. The maximum position errors in the y direction of Method 1 and K-MPC are 0.7654 and 0.337 mm, respectively. The errors of x and y direction are reduced by 37.9% and 56%, respectively.

V. Discussion

As aforementioned, the constant curvature assumption has advantages in terms of algorithm implementation and computational efficiency in comparison to other algorithms. In this paper, the constant curvature assumption is used as the basis to design the controller due to its advantages in computational efficiency and algorithm implementation. When the driving wire is tight, the relationship between the deformation angle of the continuum manipulator and the motor angle is linear, as shown in Fig. 6. After the continuum manipulator runs for a while, the driving wire could be slack. When the driving wire is slack, the above-mentioned relationship shows hysteresis, as shown in Fig. 7. It is difficult to apply a mathematical model to represent the relationship between the length of the driving wires and the motor angle as such a relationship behaves strongly nonlinear. This also explains why the control performance degrades using Method 1. To improve the control accuracy, such a nonlinear relationship is identified by the Koopman theory. Then, the system input is obtained by the MPC. Finally, when the driving wire is slack, the continuum manipulator can be controlled precisely through the K-MPC. Considering the actual operating efficiency, a selective control scheme is proposed according to the state of the driving wire.

When the driving wire is tight, the maximum and average absolute angle errors are 0.0526 and 0.0211 rad, respectively. Therefore, the Method 1 can provide a simple and efficient way for the position control of the continuum manipulator. As a data-driven approach, the K-MPC may need an additional step for data collection. Therefore, when the driving wire is tight, it is not necessary to use the Koopman theory for robot control. It is concluded from Fig.7 that the control error is large after the driving wire relaxes. When the driving wire is slack, the control comparison of Method 1, neural network, and K-MPC are given. The K-MPC algorithm uses 80 sets of data to identify the Koopman operator, and these data are also used to train the neural network. A reference trajectory (cosine function) is set to test the performance of Method 1, neural network, and K-MPC. The experimental results show that the average absolute angle errors of the above methods are 0.0594, 0.0523, and 0.0345 rad, respectively. Under the driving wire is slack, the reason for the degradation in accuracy of Method 1 is because the relationship between the length of the driving wires and the motor angle is nonlinear. Also, the small data set makes the neural network exhibit low accuracy. It can be seen from Fig. 10 that the errors at step number 12 and 50 are larger. This is mainly because the manipulator's deformation is close to 0, the driving input value of the motor cannot make the driving wire tension. In addition to the above cosine trajectory, random positions are set as the objective positions to compare Method 1 and K-MPC. Compared with Method 1, the error of K-MPC is reduced by 39%. Under the different states of the driving wire, the angle errors of different control algorithms were given in Table II to show the effectiveness of the K-MPC. The results show that the average absolute angle error of K-MPC is close to that of Method 1 when the driving wire is tight. Therefore, this selective control scheme based on the state of the driving wires is effective.

VI. Conclusion

This paper proposes a novel selective control scheme for the position control of a continuum manipulator according to the state of the driving wire. The constant curvature assumption is used as the basis to design the controller. When the state of the driving wire is tight, a linear model based on the constant curvature assumption is used to control the continuum manipulator. When the driving wires are slack, the relationship between the length of the driving wires and the motor angle is nonlinear, making the relationship between the deformation angle of the continuum manipulator and motor angle exhibit strong nonlinearity. This nonlinear relationship is difficult to be expressed by a model-based approach. Therefore, the Koopman theory is employed to linearize and represent this nonlinear relationship. Based on the linearized model constructed by the Koopman theory, the MPC is used to obtain the controller input. Furthermore, the difficulty of the Koopman theory is the design method of the lifted function. To address this difficulty, a novel design method for the lifted function is proposed based on the Legendre polynomial. A 1-DOF prototype is constructed to test the proposed selective control scheme. When the driving wire is tight, the average absolute angle error of Method 1 is 0.0211 rad. The average absolute angle error of K-MPC in the slack state of the driving wire is 0.0345 rad. These results show that the selective control scheme is effective. In the future, this selective control scheme will be applied to the multi-DOF continuum robot system.

References

[1] M. Luo, L. Liu, C. Liu, B. Li, C. Cao, X. Gao, and D. Li, "A single-chamber pneumatic soft bending actuator with increased stroke-range by local electric guidance," *IEEE Transactions on Industrial Electronics*, vol. 68, no. 9, pp. 8455–8463, 2021.

[2] S. Park, J. Kim, C. Kim, K.-J. Cho, and G. Noh, "Design optimization of asymmetric patterns for variable stiffness of continuum tubular robots," *IEEE Transactions on Industrial Electronics*, vol. 69, no. 8, pp. 8190–8200, 2022.

[3] S. Han, S. Chon, J. Kim, J. Seo, D. G. Shin, S. Park, J. T. Kim, J. Kim, M. Jin, and J. Cho, "Snake robot gripper module for search and rescue in narrow spaces," *IEEE Robotics and Automation Letters*, vol. 7, no. 2, pp. 1667–1673, 2022.

[4] H. Wang, X. Wang, W. Yang, and Z. Du, "Design and kinematic modeling of a notch continuum manipulator for laryngeal surgery," *International Journal of Control, Automation and Systems*, vol. 18, no. 11, pp. 2966–2973, 2020.

[5] S. Mbakop, G. Tagne, S. V. Drakunov, and R. Merzouki, "Parametric ph curves model based kinematic control of the shape of mobile soft manipulators in unstructured environment," *IEEE Transactions on Industrial Electronics*, vol. 69, no. 10, pp. 10 292–10 300, 2022.

[6] W. S. Rone and P. Ben-Tzvi, "Continuum robot dynamics utilizing the principle of virtual power," *IEEE Transactions on Robotics*, vol. 30, no. 1, pp. 275–287, 2014.

[7] J. Till and D. C. Rucker, "Elastic stability of cosserat rods and parallel continuum robots," *IEEE Transactions on Robotics*, vol. 33, no. 3, pp. 718–733, 2017.

[8] Z. Du, W. Yang, and W. Dong, "Kinematics modeling of a notched continuum manipulator," *Journal of Mechanisms and robotics*, vol. 7, no. 4, p. 041017, 2015.

[9] H. Wang, X. Wang, W. Yang, Z. Du, and Z. Yan, "Construction of controller model of notch continuum manipulator for laryngeal surgery based on hybrid method," *IEEE/ASME Transactions on Mechatronics*, vol. 26, no. 2, pp. 1022–1032, 2021.

[10] R. J. Webster III and B. A. Jones, "Design and kinematic modeling of constant curvature continuum robots: A review," *The International Journal of Robotics Research*, vol. 29, no. 13, pp. 1661–1683, 2010.

[11] J. Lai, K. Huang, B. Lu, Q. Zhao, and H. Chu, "Verticalized-tip trajectory tracking of a 3d-printable soft continuum robot: Enabling surgical blood suction automation," *IEEE/ASME Transactions on Mechatronics*, pp. 1–1, 2021.

[12] Y. Chen, C. Zhang, Z. Wu, J. Zhao, B. Yang, J. Huang, Q. Luo, L. Wang, and K. Xu, "The shurui system: A modular continuum surgical robotic platform for multiport, hybrid-port, and single-port procedures," *IEEE/ASME Transactions on Mechatronics*, pp. 1–12, 2021.

[13] J. H. Palep, "Robotic assisted minimally invasive surgery," *Journal of minimal access surgery*, vol. 5, no. 1, p. 1, 2009.

[14] Y. Xia and J. Wang, "A dual neural network for kinematic control of redundant robot manipulators," *IEEE Transactions on Systems, Man, and Cybernetics, Part B (Cybernetics)*, vol. 31, no. 1, pp. 147–154, 2001.

[15] L. Scimeca, J. Hughes, P. Maiolino, and F. Iida, "Model-free soft-structure reconstruction for proprioception using tactile arrays," *IEEE Robotics and Automation Letters*, vol. 4, no. 3, pp. 2479–2484, 2019.

[16] J. D. Ho, K.-H. Lee, W. L. Tang, K.-M. Hui, K. Althoefer, J. Lam, and K.-W. Kwok, "Localized online learning-based control of a soft redundant manipulator under variable loading," *Advanced Robotics*, vol. 32, no. 21, pp. 1168–1183, 2018.

[17] O. Lakhal, A. Melingui, T. M. Bieze, C. Escande, B. Conrard, and R. Merzouki, "On the kinematic modeling of a class of continuum manipulators," in *2014 IEEE International Conference on Robotics and Biomimetics (ROBIO 2014)*. IEEE, 2014, pp. 368–373.

[18] S. Boyd, S. P. Boyd, and L. Vandenberghe, *Convex optimization*. Cambridge university press, 2004.

[19] Q. Li, F. Dietrich, E. M. Bollt, and I. G. Kevrekidis, "Extended dynamic mode decomposition with dictionary learning: A data-driven adaptive spectral decomposition of the koopman operator," *Chaos: An Interdisciplinary Journal of Nonlinear Science*, vol. 27, no. 10, p. 103111, 2017.

[20] M. Korda and I. Mezić, "Linear predictors for nonlinear dynamical systems: Koopman operator meets model predictive control," *Automatica*, vol. 93, pp. 149–160, 2018.

[21] G. Mamakoukas, M. L. Castaño, X. Tan, and T. D. Murphey, "Derivative-based koopman operators for real-time control of robotic systems," *IEEE Transactions on Robotics*, vol. 37, no. 6, pp. 2173–2192, 2021.

[22] D. Bruder, X. Fu, R. B. Gillespie, C. D. Remy, and R. Vasudevan, "Koopman-based control of a soft continuum manipulator under variable loading conditions," *IEEE Robotics and Automation Letters*, vol. 6, no. 4, pp. 6852–6859, 2021.

[23] D. Bruder, R. B. Gillespie, C. D. Remy, and R. Vasudevan, "Data-driven control of soft robots using koopman operator theory," *IEEE Transactions on Robotics*, vol. 37, no. 3, pp. 948–961, 2021.

[24] M. O. Williams, I. G. Kevrekidis, and C. W. Rowley, "A data–driven approximation of the koopman operator: Extending dynamic mode decomposition," *Journal of Nonlinear Science*, vol. 25, no. 6, pp. 1307–1346, 2015.

[25] P. Qi, C. Liu, A. Ataka, H. K. Lam, and K. Althoefer, "Kinematic control of continuum manipulators using a fuzzy-model-based approach," *IEEE Transactions on Industrial Electronics*, vol. 63, no. 8, pp. 5022–5035, 2016.